Pergamon

Tetrahedron 56 (2000) 3035–3041

TETRAHEDRON

Enantiodifferentiation by Complexation with β-Cyclodextrin: Experimental (NMR) and Theoretical (MD, FEP) Studies

Dolors Salvatierra, Xavier Sánchez-Ruiz, Ramón Garduño,† Enric Cervelló, Carlos Jaime,* Albert Virgili and Francisco Sánchez-Ferrando

Department de Química, Facultat de Ciències, Universitat Autònoma de Barcelona, 08193 Bellaterra, Barcelona, Spain

Received 4 November 1999; revised 21 February 2000; accepted 2 March 2000

Abstract—Diastereomeric complexes between β-CyD and both enantiomers of mandelic acid, hexahydromandelic acid, and 1-cyclohexylethylamine were studied by NMR spectroscopy. Their inclusion complexes were studied by molecular dynamics (MD) calculations. Induced chemical shifts gave association constants of about 10^2–10^3 M^{-1}. Computed geometries for the inclusion complexes are in agreement with those deduced experimentally by NOE experiments. MD (free energy perturbation) calculations correctly predict the most stable diastereomer when enantiomers are individually complexed with β-CyD. © 2000 Elsevier Science Ltd. All rights reserved.

Introduction

Cyclodextrins (CyDs) were first isolated by Villiers,[1] but their structure remained unknown until some years later.[2] CyDs are macrocycles formed by six or more units of α-D-glucopyranose bonded through α-(1→4) bonds[3] with a known capability for forming inclusion complexes with organic compounds. Significant interest is currently centered in CyDs.[4]

Since CyDs are optically active molecules (the D-(+)-CyD is always the natural enantiomer) they can form diastereomeric pairs by complexing with racemic mixtures. This property has been used for the resolution of racemic mixtures of esters like ethylmandelates.[5,6] One of the most used applications of CyD complexes is their use as chiral shift reagents (CSR) in solution. The observation in the NMR spectrum of the two diastereomeric signals may allow quantification of the enantiomeric excess. CyDs directly compete with other CSR like lanthanide derivatives or Pirkle alcohols, and chromatography (GC[7] and HPLC[8]) using CyDs stationary phases produces enantiodifferentiation. Spectroscopic techniques, like circular dichroism,[9,10] have been utilized also to detect enantiodifferentiation. Obviously, the best proof for the enantiodifferentiation by complexing with CyDs is the isolation of crystals for each diastereoisomer.[11,12] Enantioselective reactions have also been carried out in the presence of CyDs obtaining acceptable e.e. values.[13,14]

NMR techniques are largely used for the enantiodifferentiation detection by complexing with CyDs,[15] and probably follow chromatographic studies in importance. MacNicol[16] already detected differences in the chemical shifts of the prochiral CF_3 groups from 1,1,1,3,3,3-hexafluoro-2-phenyl-2-propanol. A large number of examples can be found in the scientific literature of enantiodifferentiation detection using NMR.[17]

Molecular modeling of the enantiodifferentiation is much less developed than NMR applications.[18] Examples exist where researchers combine NMR studies with molecular modeling; menthol,[19] triptophane,[20] methyl 2-chloropropionate,[21] 1-(4-methoxybenzoyl)5-oxo-2-pyrrolidinpropanoic acid,[22] and others[23] are among the molecules studied. In a recent article,[24] Lipkowitz studied the complexation of five organic guests to permethyl-β-CyD by MD simulations; results indicated the interior of the cavity as the preferred binding site for producing enantiodifferentiation in the gas phase. The computational protocol for solving this problem has been described previously.[24]

Predicting enantioselection is a difficult task, and no studies have been made to solve this problem in aqueous solution. In this article, the inclusion complexes of six molecules (three enantiomeric pairs), *R*- and *S*-mandelic acid (**1*R*** and **1*S***), *R*- and *S*-hexahydromandelic acid (**2*R*** and **2*S***) and *R*- and *S*-1-cyclohexylethylamine (**3*R*** and **3*S***) with β-CyD are presented (Fig. 1). Complexes have been studied by NMR and MD calculations. Stoichiometry, association

Keywords: complexes; cyclodextrins; molecular modeling; molecular recognition.

* Corresponding author. Tel.: +34-9-3581-2591; fax: +34-9-3581-1265; e-mail: carlos.jaime@uab.es

† On leave of absence from Instituto de Física, Laboratorio de Cuernavaca, Universidad Nacional Autónoma de México, Cuernavaca (Morelos), México.

0040–4020/00/$ - see front matter
PII: S0040-4020(00)00192-7

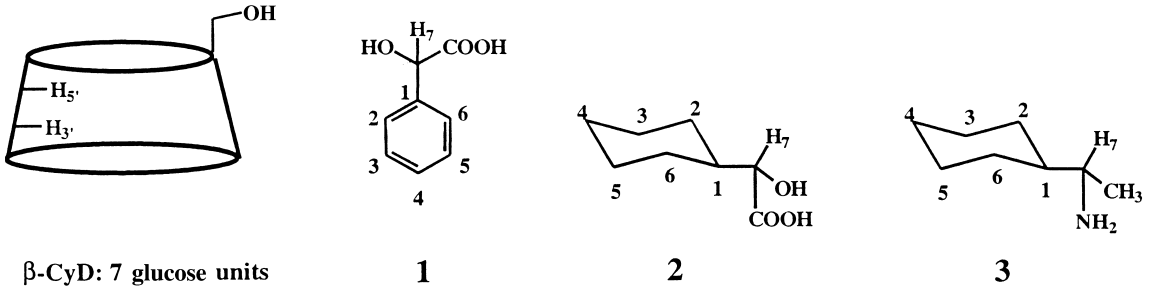

β-CyD: 7 glucose units **1** **2** **3**

Figure 1. Structures and numbering used throughout this work.

constant, and inclusion geometry for each of the complexes formed were determined, and MD simulations (FEP) correctly indicate the stability order for each enantiomeric pair studied.

Results

NMR experiments

General procedure. Fourteen samples for **1*R***, **1*S***, **2*R***, **2*S***, **3*R*** and **3*S*** with $[host]_i/[guest]_i$ ratios ranging from 12.9:0.3, 12.6:0.3, 9.5:0.4, 15.2:0.3, 7.0:0.2 and 10.0:0.2, respectively, were prepared and studied by NMR. Job's diagrams[25] indicated the formation of 1:1 complexes in all studied compounds. Association constants were determined using the induced chemical shifts for inner β-CyD protons ($H_{3'}$ and $H_{5'}$), and guest protons in conjunction with the program CALCK.[26] Selective 1D-ROESY experiments were carried out on samples of **1*R***, **1*S***, **2*R***, **2*S***, **3*R*** and **3*S*** having 1:1 host/guest ratios.

1*R*/β-CyD and 1*S*/β-CyD complexes. Job's plots indicate a 1:1 stoichiometry for both complexes with association constants of 811 and 178 M^{-1} for **1*R***/β-CyD and **1*S***/β-CyD, respectively. Results from selective 1D-ROESY experiments are shown in Table 1.

ROE signals between inner β-CyD protons and all protons of **1*R*** demonstrate the formation of an inclusion complex. Inner $H_{3'}$ protons present larger ROE effects on saturation of either H_7 or H_{Ar} guest protons than inner $H_{5'}$ protons. Compound **1*R*** is, consequently, mainly located at the wider rim of the host although ROE signals on $H_{5'}$ indicate that the guest should also be in the narrower part of the host cavity for some time. Complex **1*S***/β-CyD behaves differently. The absence of ROE signals over inner $H_{5'}$ protons on irradiation of the H_7 of **1*S*** suggests a single inclusion geometry with the stereogenic center located at the wider zone of the cavity, and the aromatic ring in the center of the cavity (presence of ROE signals with both inner protons).

2*R*/β-CyD and 2*S*/β-CyD complexes. Job's plots also indicate a 1:1 stoichiometry for both complexes. Association constants of 3812 and 1040 M^{-1} for **2*R***/β-CyD and **2*S***/β-CyD, respectively, were determined by CALCK.[26] Results from selective 1D-ROESY experiments are shown in Table 2. Larger ROE effects over $H_{3'}$ protons than over $H_{5'}$ protons on saturation of the H_7 protons of both complexes **2*R***/β-CyD and **2*S***/β-CyD are observed (Table 2), indicating more proximity between H_7 and $H_{3'}$ than between H_7 and $H_{5'}$. Saturation of equatorial and axial guest protons also produces larger ROE effects over $H_{3'}$ than over $H_{5'}$. All these results suggest that substrates **2*R*** and **2*S*** are mainly located at the wider zone of the cavity, although they should also occupy the narrower part as deduced from the observed ROE with $H_{5'}$ protons.

Table 1. Relative NOE values obtained by selective 1D-ROESY experiments for the **1*R***/β-CyD and **1*S***/β-CyD complexes. Negative signs indicate absence of NOE signal

Guest	Observed	Saturated protons			
		H_{Ar}	H_7	$H_{3'}$	$H_{5'(6')}$[a]
1*R*	H_{Ar}	(−)	0.13	0.40	
	H_7	0.20		(−)	(−)
	H_1				
	$H_{3'}$	1	1		1
	$H_{5'}$[b]	0.52	0.38	1	
1*S*	H_{Ar}		1	0.12	0.27
	H_7	0.55		0.04	(−)
	H_1				
	$H_{3'}$	1	0.98		1
	$H_{5'}$[b]	0.76	(−)	1	

[a] Both protons are irradiated due to overlapping of signals.
[b] Only $H_{5'}$ is assigned as responsible for the observed NOE due to the multiplicity of the enhanced signal (triplet).

Table 2. Relative NOE values obtained by selective 1D-ROESY experiments for the **2*R***/β-CyD and **2*S***/β-CyD complexes. Negative signs indicate absence of NOE signal

Guest	Observed	Saturated protons				
2*R*		H_7	$H_{eq,1}$	H_{ax}	$H_{3'}$	$H_{5'(6')}$[a]
	H_7		0.09	0.06	0.04	0.06
	$H_{1,2e,6e}$	0.25		1	0.15	0.01
	$H_{3e,5e}$	(−)		0.97	0.18	0.08
	H_{4e}	(−)		0.34	0.08	0.04
	H_{ax}	0.13	1		0.38	0.14
	$H_{3'}$	1	0.17	0.08		1
	$H_{5'}$[b]	0.18	0.07	0.11	1	
2*S*	H_7		0.09	0.08	0.14	0.05
	$H_{1,2e,6e}$	0.24		0.91	0.21	0.05
	$H_{3e,5e}$	(−)		1	0.23	0.13
	H_{4e}	(−)		0.43	0.12	0.04
	H_{ax}	0.16	1		0.46	0.21
	$H_{3'}$	1	0.08	0.15		1
	$H_{5'}$[b]	0.18	0.06	0.11	1	

[a] Both protons are irradiated due to overlapping of signals.
[b] Only $H_{5'}$ is assigned as responsible for the observed NOE due to the multiplicity of the enhanced signal (triplet).

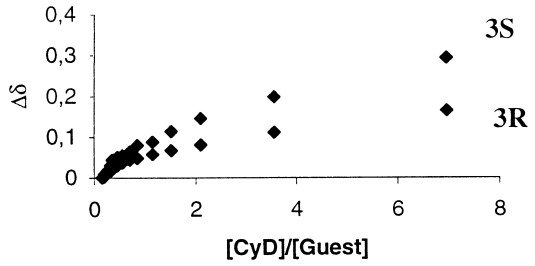

Figure 2. Graphical representations of $\Delta\delta$ versus [CyD]/[Guest] for the β-CyD complexes with **3*R*** and **3*S***.

3*R*/β-CyD and 3*S*/β-CyD complexes. Job's plots again indicate 1:1 stoichiometry for both complexes. Although CALCK could determine an association constant for **3*R***/β-CyD (with a too small value),[27] it was unable to determine that for **3*S***/β-CyD. The graphical representation of induced chemical shifts for **3*R*** and **3*S*** (Fig. 2) versus the [host]/[guest] ratio indicates very small association constants for both compounds, and none of them reach the equilibrium when the solution contains 7 equiv. of the host; nevertheless, that for **3*S*** seems to be the largest. Results from selective 1D-ROESY experiments are shown in Table 3, and are totally parallel to those for **2*R***/β-CyD and **2*S***/β-CyD complexes. Guests are mainly located at the wider part of the cavity but some occupancy of the narrower part is also necessary to explain the results.

Molecular dynamics calculations

Methodology. MD simulations were performed for each of the studied inclusion complexes. Our goal is to reproduce geometries and energies derived exclusively from inclusion processes; thus two geometries, **A** and **B** (Fig. 3), can be foreseen as the most probable for the inclusion of studied guests into the β-CyD. The starting points were obtained by extensive MM calculations using our previously described methodology[28] that considers several orientations for guests to account for bimodal complexations. The host was initially oriented and restrained as to be kept in the *XY* plane with its narrower rim in the positive *Z*-axis. Guests were located far from the host and were forced to pass across the macrocycle by gradually changing its *Z* coordinate. Three different guest orientations were considered depending on which functional group enters first into the host cavity. All these 'inclusions' give several energy minima which were fully optimized without any restriction. The two most stable structures for these inclusions were used as starting points in the MD computations. Simulations were carried out with MacroModel v4.5 and BatchMin v4.5 programs.[29] Selected force field was AMBER* (the implemented version of AMBER[30] force field), together with the GB/SA solvation model[31] to account for the solvent effect (water) on the inclusion complexes. Distances between three alternate glycosidic oxygens and the guest carbon atom carrying the substituent were restrained to prevent the host and guest from separating. A flat-bottom potential of 100 kJ mol^{-1} and a tolerance of ± 2 Å were used. Three short MD runs for heating the system from 5 to 300 K, followed by a 75 ps equilibration run, preceded the 2400 ps simulation run. Structures were saved to disk every 0.5 ps. The energy was not equilibrated until the last 1000 ps (Fig. 4); only these 2000 structures were used for the MD analysis. The trajectories were analyzed using a local program.[32]

Table 3. Relative NOE values obtained by selective 1D-ROESY experiments for the **3*R***/β-CyD and **3*S***/β-CyD complexes. Negative signs indicate absence of NOE signal

Guest	Observed	Saturated protons					
3*R*		H_7	H_{eq}	H_{ax}	H_{Me}	$H_{3'}$	$H_{5'(6')}$[a]
	H_7		0.11	0.08	0.30	0.05	(−)
	H_{eq}	0.63	1		0.85	0.19	0.09
	$H_{1,3,4,5}$	0.42		0.44	(−)	0.12	0.06
	$H_{2,6}$	0.63		1	(−)	0.14	0.05
	H_{Me}	0.70	(−)	0.14		0.12	(−)
	$H_{3'}$	1	0.40	0.22	1		1
	$H_{5'}$[b]	0.32	0.27	0.14	0.24	1	
3*S*	H_7		0.06[c]	0.06	0.53	0.06	(−)
	$H_{1,eq}$	0.60		1	1	0.21	0.11
	H_{ax}	0.39	1[c]		(−)	0.10	0.07
	H_{Me}	0.83	(−)	(−)		0.14	(−)
	$H_{3'}$	1	0.18[c]	0.16	0.79		1
	$H_{5'}$[b]	0.27	0.12[c]	0.09	0.21	1	

[a] Both protons are irradiated due to overlapping of signals.
[b] Only $H_{5'}$ is assigned as responsible for the observed NOE due to the multiplicity of the enhanced signal (triplet).
[c] Protons H_1 and H_{eq} are irradiated due to overlapping of signals.

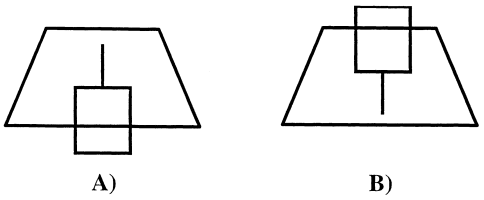

Figure 3. Schematic representation of the two most probable inclusion geometries used as starting point in the MD simulations.

The final goal is to compare the experimental with computed interatomic distances to deduce the most probable geometry for inclusion complexes. The well-known dependence[33] of NOE on $(R_{ij})^{-6}$ allows one to obtain the experimental distance ratios by simply dividing NOE values: $(\eta_{ab}/\eta_{bc})=(R_{ab}/R_{bc})^{-6}$. However, when in the studied system several equivalent protons (i.e. seven in the β-CyD) exist, the use of 'effective' distances is needed. 'Effective' distances are those averaged taking into account all the equivalent protons giving rise to one NOE signal. Those distances are obtained by using Bendall's equation[34] (Eq. (1)) originally deduced to account for the rotamer

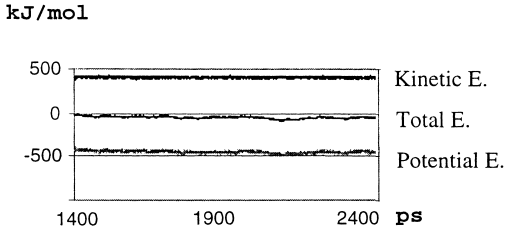

Figure 4. Variation of energy in the last 1000 ps of the MD simulation of the **1*R***/β-CyD complex considered in orientation **A** (see Fig. 3).

Table 4. Experimental NOE ratios, computed 'effective' distance ratios and root-mean-square (rms) values for **1*R***/β-CyD and **1*S***/β-CyD complexes in orientations **A** and **B**

Compound	Orientation	Computed 'effective' distance ratio[a]				Root-mean-square (rms)
		3′,Ar/5′,Ar	3′,7/5′,7	Ar,3′/5′,3′	Ar,5′/3′,5′	
1*R*	**A**	1.057	1.020	1.156	1.093	0.174
	B	1.096	1.046	1.256	1.146	0.158
	NOE	0.897	0.851	1.403	1.165	
1*S*	**A**	1.047	0.975[b]	1.143	1.092	0.181
	B	1.015	0.746[b]	1.103	1.086	0.186
	NOE	0.955	0.833[b]	1.424	1.244	

[a] 3′,Ar/5′, Ar indicates the effective distance between $H_{3'}$ and H_{Ar} divided by effective distance between $H_{5'}$ and H_{Ar}. However, the corresponding experimental distance ratio is obtained by dividing the experimental NOE for $H_{5'}$ by that for $H_{3'}$ on irradiation of H_{Ar} protons to the 1/6 power.
[b] Values corresponding to Ar, 3′/7,3′ because $H_{5'}$ does not present NOE signal on irradiation of H_7 (see Table 1).

contribution:

$$1/R_{\text{eff}}^6 = 1/n \sum (1/R_i^6) \qquad (n = 7) \tag{1}$$

The final 'effective' distance was computed by considering all collected samplings from the last equilibrated 1000 ps. Experimental NOEs are exclusively observed between nuclei separated less than 3.5 Å. Therefore, those computed interproton distances larger than 4 Å were discarded.

1*R*/β-CyD and 1*S*/β-CyD complexes. ROESY experiments (vide supra) do not indicate a single complexation geometry for the inclusion of **1*R*** but suggest a preference for type **B** complex (Fig. 3) in the case of **1*S***. Table 4 contains the ratio between computed 'effective' distances together with some experimentally obtained NOE ratios for both complexes. Root-mean-square (rms) comparison between computed and experimental distance ratios predicts a small preference for orientation **B** for the complex of **1*R*** (**A**=0.174, **B**=0.158), whereas for **1*S*** both orientations give the same deviation (**A**=0.181, **B**=0.186). The $H_{3'}/H_{5'}$ distance is almost fixed (2.650 Å) because both are axial protons in the pyranose rings. Ratios considering this distance should thus be more reliable than other ratios containing more variable interproton distances. Computed rms values for **1*R*** are transformed now to 0.182 and 0.105 for **A** and **B** complexes, respectively. Compound **1*S*** gives now rms values of 0.225 and 0.253 for **A** and **B**, respectively. No clear preference for any orientation can be predicted in any case.

2*R*/β-CyD and 2*S*/β-CyD complexes. ROESY experiments (vide supra) do not suggest a single complexation geometry either for the inclusion of **2*R*** or for **2*S***. Table 5 contains the ratio between computed 'effective' distances together with some of the experimentally obtained NOE ratios for both complexes.

The computed 'effective' distance between H_7 and $H_{5'}$ protons for **2*R*** in orientation **B** is 5.706 Å, too large to predict NOE between these two protons. This fact suggests that **2*R*** should adopt orientation **A** exclusively, in contradiction with the experimental data. The computed 'effective' distances between H_7 and $H_{5'}$ and $H_{3'}$ (3.604 and 3.877 Å, respectively) suggest slightly larger NOE for $H_{5'}$ than for $H_{3'}$ on saturation of H_7, while experiments show larger NOE for $H_{3'}$ than for $H_{5'}$ (1 and 0.18, respectively). Most likely, the observed NOE would arise from **A** and **B** complexes simultaneously. The NOE between $H_{3'}$ and H_7 comes from orientation **B** (R_{eff}=2.855 Å) while that between $H_{5'}$ and H_7 comes from orientation **A** (R_{eff}= 3.604 Å).

The situation is again similar for compound **2*S***. Long computed 'effective' distances are obtained in both orientations (see Table 5). It is thus necessary to consider both geometries simultaneously to explain the experimentally

Table 5. Experimental NOE ratios, computed 'effective' distances ratios and root-mean-square (rms) values for **2*R***/β-CyD and **2*S***/β-CyD complexes in orientations **A** and **B**

Compound	Orientation	Computed 'effective' distance ratios[a]					Root-mean-square (rms)
		3′,7/5′,7	7,3′/5′,3′	7,5′/3′,5′	4e,3′/5′,3′	4e,5′/3′,5′	
2*R*	**A**	1.076	1.516	1.409	1.290	1.290	0.286
	B	–[b]	1.117	–[b]	1.281	1.281	0.445
	NOE	0.751	1.710	1.593	1.523	1.711	
2*S*	**A**	–[c]	–[d]	1.422	1.305	1.305	0.284
	B	–[c]	1.339	–[c]	1.144	1.144	0.445
	NOE	0.751	1.710	1.593	1.523	1.711	

[a] 3′,7/5′,7 Indicates the effective distance between $H_{3'}$ and H_7 divided by effective distance between $H_{5'}$ and H_7. The corresponding experimental distance ratio is obtained by dividing the experimental NOE for $H_{5'}$ by that for $H_{3'}$ on irradiation of H_7 protons to the 1/6 power.
[b] Computed effective distance between H_7 and $H_{5'}$ is 5.706 Å; no NOE should be observed.
[c] Computed effective distance between H_7 and $H_{5'}$ is 7.183 Å; no NOE should be observed.
[d] Computed effective distance between H_7 and $H_{3'}$ is 6.196 Å; no NOE should be observed.

Table 6. Experimental NOE ratios, computed 'effective' distance ratios and root-mean-square (rms) values for **3*R***/β-CyD and **3*S***/β-CyD complexes in orientations **A** and **B**

Compound	Orientation	Computed 'effective' distance ratios[a]						Root-mean-square (rms)
		3′,7/5′,7	7,3′/5′,3′	2a,3′/5′,3′	2a,5′/3′,5′	Me,3′/5′,3′	3′,Me/5′,Me	
3*R*	**A**	1.127	1.306	1.185	1.181	1.329	1.139	0.312
	B	1.030	1.183	1.237	1.116	1.177	0.973	0.326
	NOE	0.827	1.627	1.388	1.648	1.424	0.788	
3*S*	**A**	0.997	1.169	1.286	1.127	1.176	0.970	0.298
	B	0.997	1.230	1.211	1.113	1.173	0.952	0.288
	NOE	0.804	1.598	1.388	1.468	1.558	0.802	

[a] 3′,7/5′,7 Indicates the effective distance between $H_{3'}$ and H_7 divided by effective distance between $H_{5'}$ and H_7. However, the corresponding experimental distance ratio is obtained by dividing the experimental NOE for $H_{5'}$ by that for $H_{3'}$ on irradiation of H_7 protons to the 1/6 power.

obtained NOE values. Proton H_7 is near $H_{3'}$ protons only in orientation **B**, but it is only near $H_{5'}$ in orientation **A**. The smaller rms for orientation **A** is suggesting a preference for this orientation.

3*R*/β-CyD and 3*S*/β-CyD complexes. ROESY experiments (vide supra) do not suggest a single complexation geometry either for the inclusion of **3*R*** or for **3*S***. Table 6 contains the ratio between computed 'effective' distances together with the experimentally obtained NOE ratios for both complexes.

All guest protons of **3*R*** and **3*S*** give NOE signals either with $H_{3'}$ or with $H_{5'}$. These experimental facts are corroborated by MD simulations (all computed 'effective' distances are smaller than 3.1 Å). Nevertheless, the agreement between computed structures and experimental distance ratios is rather poor (rms around 0.3 Å). Table 6 indicates that while some computed ratios are closer to the experimental ones in orientation **A**, the others are closer in **B**. Both orientations are thus needed to explain satisfactorily the experimental results.

Free energy perturbation studies. Free energy perturbation (FEP) calculations have been applied to a large number of chemical problems.[35] The thermodynamic cycle shown in Fig. 5 was considered.

Values for ΔG_1 and ΔG_3 are obtained experimentally from association constants (K_1 and K_3), and ΔG_4 is zero if we assume that each enantiomer (*R* or *S*) is far enough from the host (CyD) as not to interact. Under these considerations, ΔG_2 can be obtained from the FEP calculations, and it should be equal to $\Delta G_2 = RT \ln K_1/K_3$.

Free energy perturbations were initially performed using MacroModel and BatchMin v4.0 packages.[29] Extremely long computer times were needed and results presenting a large hysteresis were obtained. A change of the program was required and new FEPs were performed using the original AMBER[30] program extended with the glycam_93[36] parameter set for oligosaccharides. Atomic charges for the studied guests were obtained by using the option QMPEP in MOPAC-93.[37] The most stable structures for each **A** and **B** orientations obtained in MM calculations were used as the starting points. Explicit solvent molecules (TIP3P water) with periodic boundary conditions (constant pressure at 1 atm) were used to model the effect of solvent. Two short MD runs (10 ps) were needed to equilibrate the system prior to the FEP computations. Classical MD with the window perturbation method was used at 298 K with SHAKE option active for hydrogen atoms. Several runs using different conditions were performed to compute the FEP values but the density of the system was either too unstable or unreliable. Only when mutations were carried out in 201 windows of 2 ps using 1000 equilibration steps and 1000 samplings per window with time step of 0.1 fs and a lambda increment of 0.005, density was stable and presented reasonable values. Double-wide sampling was used.

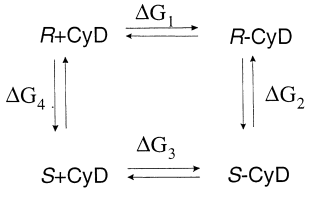

Figure 5. Thermodynamic cycle considered to perform the free energy perturbation calculations. ΔG_1 and ΔG_3 are experimentally deduced, ΔG_4 is zero, and ΔG_2 is computed by FEP calculations.

Table 7 contains the results from the FEP calculations. Enantiodifferentiation of mandelic acid **1** is computed to be due to both orientations **A** and **B**. The experimental ΔG_2 is perfectly matched if the average of the two values is considered. However, this suggests that both orientations are equally populated for each enantiomer, but our MD simulations indicate **1*R*** ($E_{total} = -24566.3$ kJ mol^{-1}) is more stable than **1*S*** ($E_{total} = -24508.6$ kJ mol^{-1}) in orientation **A**, while **1*S*** ($E_{total} = -25422.3$ kJ mol^{-1}) predominates over **1*R*** ($E_{total} = -25317.0$ kJ mol^{-1}) in orientation **B**. Enantiodifferentiation for hexahydromandelic acid **2** is computed to be due to orientation **A**. The computed mutation of **3*R*** into **3*S*** shows a very similar preference of **3*S*** for both orientations **A** and **B**.

Discussion

The presence of experimental NOE signals between all inner β-CyD protons and all guest protons is a definite proof of the existence of inclusion complexation. Observed NOEs are always greater for $H_{3'}$ than for $H_{5'}$. This fact indicates that guests are usually located at the wider part of the CyD cavity.

Table 7. Density (in g dm^{-3}), computed free energies (FEP, in kJ mol^{-1}) and experimentally deduced complexation free energies (ΔG_2=RT ln K_1/K_3, in kJ mol^{-1}) for the mutation of *R* into *S* enantiomers of complexes of **1**–**3** with β-CyD

Process	Orientation	FEP				
		Density	Forward	Reverse	Average	Exp ΔG_2
1*R*→1*S*	**A**	1.025±0.003	1.42	0.84	0.59	
	B	1.016±0.007	7.59	−6.77	7.19	3.44
2*R*→2*S*	**A**	1.013±0.003	4.39	−3.39	3.89	
	B	1.014±0.004	−0.42	−1.30	0.10	3.21
3*R*→3*S*	**A**	1.016±0.005	−5.56	5.02	−5.27	
	B	1.007±0.004	−5.27	6.19	−5.73	–[a]

[a] Inconclusive; experimental *K*s are very small, see text.

The large dispersion and similarity between all observed NOE values introduce difficulty, or even impossibilities, in assessing a single complexation geometry. This fact, together with the relatively low association constants for most of the studied complexes, makes us consider that the inclusion process is too fast to be studied exclusively through NMR experiments. Observed NOE values are a weighted average from **A** and **B** inclusion geometries, both having different stabilities.

Comparison of the experimentally deduced distances based on NOE values with computed 'effective' distances from MD simulations allows us to confirm that no single geometry for the inclusion complexation can be suggested, but rather both **A** and **B** coexist. Nevertheless, researchers should notice that an NOE ratio of 2:3 implies a distance ratio of $(1/2)^{1/6}$:$(1/3)^{1/6}$ (i.e. 0.891:0.833), respectively. These two values are practically identical, and distances between involved protons are also very similar. Only when the NOE ratio is 20:30, is the distance ratio transformed into 0.60:0.57, i.e. the distance separating one pair of protons is twice the distance separating the second pair. Our observed NOE ratios are smaller than 2, it is thus understandable why many geometries will correlate with experimental values.

The free energy perturbation method applied to the study of the inclusion complexes has proven to be efficient in qualitatively reproducing the experimentally obtained free energy differences. This point is of great importance for the studies of chiral recognition through NMR experiments using CyDs as hosts. Let us consider a racemic mixture. If the chiral recognition by CyDs is carried out, and association constants for the CyD complex of each individual enantiomer can be determined, it should not then be necessary to resolve enantiomers (not always an easy task) to know which is responsible for each signal: computation of the FEP for the enantiomer mutation would give which one binds with the larger energy exchange, i.e. the larger association constant. Nevertheless, a correct correlation with three compounds could be considered as fortuitous. More work on this point is necessary before being able to quantitatively interpret the FEP results.

Conclusions

The inclusion complexes between β-CyD and individual enantiomers of **1**, **2** and **3** do not exclusively adopt a single geometry but are very likely to exist as an average between two different orientations (**A** and **B**), exchanging very rapidly as deduced from NMR experiments and MD simulations. The free energy perturbation method used in this work correctly predicts the sign of the $\Delta\Delta G$ for the complexation of two enantiomers with a chiral host like β-CyD, and opens possibilities for deducing which enantiomer is the best complexed. Enantiodifferentiation of hexahydromandelic acid is due to orientation **A**, while both orientations **A** and **B** contribute to that of mandelic acid and 1-cyclohexylethylamine.

Experimental

All chemicals were purchased from Aldrich. Solutions of 1.63×10^{-2} M of β-CyD and of compounds **1**–**3** in D_2O were prepared with the help of sonication. Samples were prepared by mixing variable volumes of host and guest solutions. NMR spectra were obtained on a Bruker AMX-400 machine at 300 K in D_2O as the solvent. Cross-relaxation was achieved using a low-power off-resonance continuous-wave irradiation (2.5 kHz) as a mixing time during 700 ms. 1D-ROESY spectra were acquired with 1024 scans using a relaxation period of 1 s.

Acknowledgements

Financial support from DGICYT and DGES (MEC, Spain) through projects nos. PB92-0611 and PB96-1181 is gratefully acknowledged. CIRIT-CICYT and UAB are thanked for fellowships to X. S.-R. and E. C. DGU (Generalitat de Catalunya, Spain) provided a visiting professor position to R. G. MD simulations were performed on the CESCA-CEPBA resources coordinated by C^4.

References

1. Villiers, A. *C. R. Acad. Sci.* **1891**, *112*, 536–538.
2. Schardinger, F. *Wien. Klin. Wochenschr.* **1904**, *17*, 207–208.
3. Freudenberg, K.; Meyer-Delius, M. *Ber. Dtsch. Chem. Ges.* **1938**, *71*, 1596–1600.
4. A special issue of *Chem. Rev.* has recently been published dedicated to CyDs. D'Souza, V. T., Lipkowitz, K. B. (Eds.) *Chem. Rev.* **1998**, *98* (5), all pages.
5. Cramer, F. *Chem. Ber.* **1953**, *86*, 1576–1578.

6. Cramer, F.; Dietsche, W. *Chem. Ber.* **1959**, *92*, 378–384.
7. As a good review see: Schurig, V.; Nowotny, H.-P. *Angew. Chem., Int. Ed. Engl.* **1990**, *29*, 939–1076.
8. Camilleri, P.; Edwards, A. J.; Rzepa, H. S.; Green, S. M. *J. Chem. Soc., Chem. Commun.* **1992**, 1122–1124.
9. Eliseev, A. V.; Iacobucci, G. A.; Khanin, N. A.; Menger, F. M. *J. Chem. Soc., Chem. Commun.* **1994**, 2051–2052.
10. Kano, K. *J. Inclusion Phenom.* **1990**, 243–252.
11. Harata, K. *J. Chem. Soc., Perkin Trans. 2* **1990**, 799–804.
12. Hamilton, J. A.; Chen, L. *J. Am. Chem. Soc.* **1988**, *110*, 4379–4391 (and 5833–5841).
13. Coates, J. H.; Easton, C. J.; van Eyk, S. J.; May, B. L.; Singh, P.; Lincoln, S. F. *J. Chem. Soc., Chem. Commun.* **1991**, 759–760.
14. Fornasier, R.; Reniero, F.; Scrimin, P.; Tonellato, U. *J. Chem. Soc., Perkin Trans. 2* **1987**, 193–196.
15. Schneider, H.-J.; Hacket, F.; Rüdiger, V.; Ikeda, H. *Chem. Rev.* **1998**, *98*, 1755–1785.
16. MacNicol, D. D.; Kinns, M. E. *Tetrahedron Lett.* **1977**, *25*, 2173–2176.
17. (a) Greatbanks, D.; Pickford, R. *Magn. Res. Chem.* **1987**, *25*, 208–215. (b) Casy, A. F.; Mercer, A. D. *Magn. Res. Chem.* **1988**, *26*, 765–774. (c) Dodziuk, H.; Sitkowski, J.; Stefaniak, L.; Jurczak, J.; Sybilska, D. *Supramol. Chem.* **1993**, *3*, 79–81. (d) Galons, H.; Gnaïm, J.; Rysanek, N.; LeBas, G.; Villain, F.; Tsoucaris, G. *Tetrahedron: Asymmetry* **1993**, *4*, 181–184. (e) Botsi, A.; Yannakopolou, K.; Hadjoudis, E.; Perly, B. *J. Chem. Soc., Chem. Commun.* **1993**, 1085–1086. (f) Bates, P. S.; Kataky, R.; Parker, D. *J. Chem. Soc., Perkin Trans. 2* **1994**, 669–675. (g) Colquhoun, I. J.; Goodfellow, B. J. *J. Chem. Soc., Perkin Trans. 2* **1994**, 1803–1807. (h) Uccello-Barretta, G.; Balzano, F.; Caporusso, A. M.; Iodice, A.; Salvadori, P. *J. Org. Chem.* **1995**, *60*, 2227–2231. (i) Redondo, J.; Frigola, J.; Torrens, A.; Lupón, P. *Magn. Res. Chem.* **1995**, *33*, 104–109. (j) Bonomo, R. P.; Cucinotta, V.; D'Allessandro, F.; Impellizzeri, G.; Maccarrone, G.; Rizzarelli, E.; Vecchio, G. *J. Inclusion Phenom.* **1993**, *15*, 167–180. (k) Cucinotta, V.; D'Allessandro, F.; Impellizzeri, G.; Vecchio, G. *J. Chem. Soc., Chem. Commun.* **1992**, 1743–1745.
18. Lipkowitz, K. B. *Chem. Rev.* **1998**, *98*, 1829–1873.
19. Coleman, A. W.; Tsoucaris, G.; Parrot, H.; Galons, H.; Miocque, M.; Perly, B.; Keller, N.; Charpin, P. *J. Chromatogr.* **1988**, *450*, 175–182.
20. Lipkowitz, K. B.; Raghothama, S.; Yang, J. *J. Am. Chem. Soc.* **1992**, *114*, 1554–1562.
21. Köhler, J. E. H.; Hohla, M.; Richters, M.; König, W. A. *Angew. Chem., Int. Ed. Engl.* **1992**, *31*, 319–320.
22. Amato, M. E.; Lombardo, G. M.; Pappalardo, G. C.; Scarlata, G. *J. Mol. Struct.* **1995**, *350*, 71–82.
23. (a) Amato, M. E.; Djedaïni, F.; Pappalardo, G. C.; Scarlata, G. *J. Pharm. Sci.* **1992**, *81*, 1157–1163. (b) Amato, M. E.; Dejdaïni-Pilard, F.; Perly, B.; Scarlata, G. *J. Chem. Soc., Perkin Trans. 2* **1992**, 2065–2069. (c) Amato, M. E.; Pappalardo, G. C.; Perly, B. *Magn. Res. Chem.* **1993**, *31*, 455–460.
24. Lipkowitz, K. B.; Coner, R.; Peterson, M. A.; Morreale, A.; Shackelford, J. *J. Org. Chem.* **1998**, *63*, 732–745.
25. Job, P. *Ann. Chim.* **1928**, *9*, 113–125.
26. Salvatierra, D.; Díez, C.; Jaime, C. *J. Inclusion Phenom.* **1997**, *27*, 215–231.
27. A value of 37 M^{-1} was determined.
28. (a) Jaime, C.; Redondo, J.; Sánchez-Ferrando, F.; Virgili, A. *J. Org. Chem.* **1990**, *55*, 4773–4776. (b) Redondo, J.; Jaime, C.; Virgili, A.; Sánchez-Ferrando, F. *J. Mol. Struct.* **1991**, *248*, 317–329. (c) Fotiadu, F.; Fathallah, M.; Jaime, C. *J. Inclusion Phenom.* **1993**, *16*, 55–62. (d) Fathallah, M.; Fotiadu, F.; Jaime, C. *J. Org. Chem.* **1994**, *59*, 1288–1293. (e) Pérez, F.; Jaime, C.; Sánchez-Ruiz, X. *J. Org. Chem.* **1995**, *60*, 3840–3845. (f) Ivanov, P. M.; Jaime, C. *Anal. Química, Int. Ed.* **1996**, *92*, 13–16. (g) Ivanov, P. M.; Jaime, C. *J. Mol. Struct.* **1996**, *377*, 137–147. (h) Salvatierra, D.; Ivanov, P. M.; Jaime, C. *J. Org. Chem.* **1996**, *61*, 7012–7017. (i) Salvatierra, D.; Jaime, C.; Virgili, A.; Sánchez-Ferrando, F. *J. Org. Chem.* **1996**, *61*, 9578–9581. (j) Entrena, A.; Jaime, C. *J. Org. Chem.* **1997**, *62*, 5923–5927. (k) Cervelló, E.; Jaime, C. *J. Mol. Struct. (Theochem)* **1998**, *428*, 195–201. (l) Sánchez-Ruiz, X.; Ramos, M.; Jaime, C. *J. Mol. Struct.* **1998**, *442*, 93–101. (m) Cervelló, E.; Jaime, C. *Anal. Quím. Int. Ed. 1998*, *4/5*, 244–249.
29. Mohamadi, F.; Richards, N. G. J.; Guida, W. C.; Liskamp, R.; Caufield, C.; Chang, G.; Hendrickson, T.; Still, W. C. *J. Comput. Chem.* **1990**, *11*, 440–467.
30. (a) Pearlman, D. A.; Case, D. A.; Caldwell, J. C.; Seibel, G. L.; Singh, U. C.; Weiner, P.; Kollman, P. A.; AMBER version 4.0, University of California, San Francisco, 1991. (b) Weiner, S. C.; Kollamn, P. A.; Nguyen, D. T.; Case, D. A. *J. Comput. Chem.* **1986**, *7*, 230–252.
31. Still, W. C.; Tempczyk, A.; Hawley, R. C.; Hendrickson, T. *J. Am. Chem. Soc.* **1990**, *112*, 6127–6129.
32. Program ANAMD (ANAlyze Molecular Dynamics) is available from the authors on request.
33. Neuhaus, D.; Williamson, M. P. *The Nuclear Overhauser Effect in Structural and Conformational Analysis*, VCH: New York, 1989.
34. Pegg, D. T.; Bendall, M. R.; Droddell, M. R. *Aust. J. Chem.* **1980**, *33*, 1167–1170.
35. (a) Bash, P. A.; Singh, U. C.; Langridge, R.; Kollman, P. A. *Science* **1987**, *236*, 564–568. (b) McDonald, D. Q.; Still, W. C. *J. Am. Chem. Soc.* **1996**, *118*, 2073–2077. (c) Sun, Y.-C.; Veenstra, D. L.; Kollman, P. A. *Protein Eng.* **1996** *9*, 273–281. (d) Worth, G. A.; Richards, W. G. *J. Am. Chem. Soc.* **1994**, *116*, 239–250. (e) Thomas, B. E., IV; Kollman, P. A. *J. Am. Chem. Soc.* **1994**, *116*, 3449–3452. (f) Fox, T.; Thomas, B. E., IV; McCarrick, M.; Kollman, P. A. *J. Phys. Chem.* **1996**, *100*, 10779–10783. (g) Rastelli, G.; Thomas, B.; Kollman, P. A.; Santi, D. V. *J. Am. Chem. Soc.* **1995**, *117*, 7213–7227. (h) Morgantini, P-Y.; Kollman, P. A. *J. Am. Chem. Soc.* **1995**, *117*, 6057–6063. (i) Wong, C. F.; McCammon, A. *J. Am. Chem. Soc.* **1986**, *108*, 3830–3832. (j) Jorgensen, W. L.; Boudon, S.; Nguyen, T. B. *J. Am. Chem. Soc.* **1989**, *111*, 755–757. (k) Rao, S. N.; Singh, U. C.; Bash, P. A.; Kollman, P. A. *Nature* **1987**, *328*, 551–554. (l) Mark, A. E.; van Helden, S. P.; Smith, P. E.; Janssen, L. H. M.; van Gunsteren, W. F. *J. Am. Chem. Soc.* **1994**, *116*, 6293–6302. (m) Singh, U. C.; Brown, F. K.; Bash, P. A.; Kollman, P. A. *J. Am. Chem. Soc.* **1987**, *109*, 1607–1614.
36. Woods, R. J.; Dwek, R. A.; Edge, C. J.; Fraser-Reid, B. *J. Phys. Chem.* **1995**, *99*, 3832–3846.
37. Stewart, J. J. P. Fujitsu Limited, Tokyo, Japan; 1993.